

Catalysis Science & Technology

Accepted Manuscript



This is an *Accepted Manuscript*, which has been through the Royal Society of Chemistry peer review process and has been accepted for publication.

Accepted Manuscripts are published online shortly after acceptance, before technical editing, formatting and proof reading. Using this free service, authors can make their results available to the community, in citable form, before we publish the edited article. We will replace this *Accepted Manuscript* with the edited and formatted *Advance Article* as soon as it is available.

You can find more information about *Accepted Manuscripts* in the [Information for Authors](#).

Please note that technical editing may introduce minor changes to the text and/or graphics, which may alter content. The journal's standard [Terms & Conditions](#) and the [Ethical guidelines](#) still apply. In no event shall the Royal Society of Chemistry be held responsible for any errors or omissions in this *Accepted Manuscript* or any consequences arising from the use of any information it contains.

Cite this: DOI: 10.1039/c0xx00000x

www.rsc.org/xxxxxx

ARTICLE TYPE

Study of the Local Structure and Oxidation State of Iron in Complex Oxide Catalysts for Propylene Ammoxidation

Li-bin Wu^{a,b}, Liang-hua Wu^a, Wei-min Yang^{a,*} and Anatoly I. Frenkel^{b,*}

Received (in XXX, XXX) Xth XXXXXXXXXX 20XX, Accepted Xth XXXXXXXXXX 20XX

DOI: 10.1039/b000000x

Iron molybdate plays crucial role in the complex oxide catalysts used for selective oxidation and ammoxidation of hydrocarbons but its structural and electronic properties, and their changes in the process of the reaction are poorly understood. A combined use of Raman, X-ray absorption, and UV-visible spectroscopies was applied to investigate a commercial catalyst as a function of the reaction time. The results show that an iron-containing compound has existed as predominantly ferric molybdate in the fresh catalyst, which reduced progressively in the process of reaction and formed predominantly ferrous molybdate. The irreversible transformation from $\text{Fe}_2(\text{MoO}_4)_3$ toward FeMoO_4 was accompanied by formation of small amount of Fe_2O_3 . These two processes observed in our experiment shed light on the deactivation mechanism of this complex catalyst because they have negative effect on the selectivity and activity. Specifically, they are responsible for the deterioration of the redox couple, blocking the transmission of lattice oxygen, and irreversibly changing the catalyst structure. Based on the results of the combined techniques, a refined procedure has been proposed to develop more stable and efficient selective oxidation catalyst.

1. Introduction

Selective catalytic oxidation and ammoxidation of hydrocarbons are used in approximately one quarter of the most important industrial chemicals and basic intermediates produced by all catalytic processes worldwide.¹ Molecular-level understanding of catalytic behaviors in these processes is important for advancing the general knowledge of catalytic mechanisms and forming a basis for rational design of new catalysts and processes. A major breakthrough in the development of catalysts for oxidation and ammoxidation of olefins was the discovery of the promoting action of iron in the bismuth phosphomolybdate catalyst.^{2,3} Although a number of other elements such as Ni, Co, Cr, Mn, and K were later introduced to form the most efficient multicomponent molybdate (MCM) catalyst,⁴ iron continued to be an important promoter in both molybdenum- and antimony-based catalysts.⁵ Different chemical forms of iron in molybdate catalysts and its role as a promoter has become subjects of intense research.⁶ Early studies by Annenkova, et al⁷ revealed that $\text{Bi}_2(\text{MoO}_4)_3$, $\text{Fe}_2(\text{MoO}_4)_3$, and $\text{Bi}_2\text{Fe}_4\text{O}_9$ are the main components in a Fe-Mo-Bi ternary system. Batist, et al⁸ reported the formation of $\text{Bi}_3\text{FeMo}_2\text{O}_{12}$ in another Fe-Mo-Bi type system. Wolf and Matura concluded that maximum activity and selectivity of the $\text{Mg}_{7/1-x}\text{Fe}_x\text{Mo}_{12}\text{BiO}_n$ ($0 \leq x \leq 4$) catalyst is displayed when $x = 2.5$ but did not explain the significance of this optimum iron concentration.⁹ Van Oeffelen arrived at the conclusion that the role of iron in the same system is to maintain Bi in oxidized state, by functioning as a redox couple and to account for the optimum iron level at $x = 2.5$.¹⁰ Consequently, an equation of $\text{Bi}^{0+} + 3\text{Fe}^{3+}$

$\rightarrow \text{Bi}^{3+} + 3\text{Fe}^{2+}$ was proposed. The role of iron as redox $\text{Fe}^{3+}/\text{Fe}^{2+}$ couple was again discussed by Batist.¹¹ Apart from functioning as redox couple, iron could also be involved in the formation of other important compounds (as in the case of bismuth molybdate) which can display good activity, selectivity and stability by stabilizing the structure of catalysts.¹²

The time-dependent changes in the catalyst's composition offer a possible clue towards the explanation of the deterioration of its catalytic activity. Deactivation of MCM catalyst was attributed to the structural transformation of iron-molybdate due to the loss of MoO_3 by volatilization.¹³ MoO_3 is mainly formed by reduction of $\text{Fe}_2(\text{MoO}_4)_3$ in the redox catalytic process according to the equation: $\text{Fe}_2(\text{MoO}_4)_3 \rightarrow 2\text{FeMoO}_4 + \text{MoO}_3 + [\text{O}]_{\text{Lattice}}$, which was evidenced by the presence of a mixture of $\text{Fe}_2(\text{MoO}_4)_3$ and Fe_2O_3 in similar catalysts.¹⁴ The iron oxide formed by oxidation of the ferrous molybdate promotes propylene deep oxidation, deterioration of catalyst activity, target product degradation and is responsible for the reddish-brown color of the spent MCM catalysts. Additionally, the increasing loss of reversible $\text{Fe}^{3+}/\text{Fe}^{2+}$ redox couple or $\text{Fe}_2(\text{MoO}_4)_3$ structure collapse can also lead to other adverse consequences, such as the increasing pressure drop in the catalytic bed, degradation of the catalyst mechanical resistance, and the decreasing residual activity of MCM.¹⁵

It is evident from the prior results that the main challenge towards better understanding the role of iron in this important class of catalysts is the heterogeneity of the chemical states of iron, the coordination environments around iron atoms, as well as their changes during the reaction. This complexity presents

significant challenges for their structural and chemical analyses due to the ensemble-average nature of most characterization techniques. In this work, we report a combined use of X-ray absorption fine structure (XAFS) spectroscopy, Raman spectroscopy and diffuse reflectance UV-visible light (DR-UV-vis) spectroscopy, for determining the dominant chemical states and functional forms of Fe, and their change during the reaction process in a representative commercial catalyst. The methods used in our work were found to be useful for multi-technique studies of complex catalysts.^{16,17} XAFS is known for its excellent sensitivity to chemistry and coordination environments of iron complexes,¹⁸ and it is used extensively for analysis of degradation in MCM catalysts. Similar to other ensemble-average techniques such as XRD, XAFS is not sensitive to minority species because it is a volume-average method. Raman spectroscopy, on another hand, is capable of detecting such species due to various selection rules.¹⁹ For example, small amounts of MoO₃ mixed into a ferric molybdate-rich phase may not be detectable by XAFS or XRD, but would be detectable by Raman spectroscopy which is used extensively for studying structure of molybdates.²⁰ In addition, the fact that the reduction form of iron molybdate, iron oxide, has no significant contribution to Raman spectrum due to its weak Raman scatter and is sensitive to DR-UV-vis spectroscopy, should also be taken into consideration.

Another important aspect of catalysis investigations that this work helps resolve is the issue of heterogeneity of different chemical forms of the same element in the sample. Average techniques such as XAFS, used alone, cannot discriminate between the different models: 1) changes in the chemical states of Fe occur uniformly throughout the entire sample or 2) the sample has a mixture of the same two or more states of Fe at all times, and the volume fraction of each state changes with time.

Our work shows that correlating the results of these techniques is required in order to resolve this challenge and propose a specific model of chemical and structural transformation in iron species and shed light on the mechanism of the catalyst deactivation.

2. Experimental

2.1 Catalyst preparation and catalytic tests

The catalyst in this study is a member of family Bi_{0.5-1}Fe₂₋₃Mo₁₂₋₁₄X_mO₄₀₋₅₀,^{21,22} (denoted hereafter as Fe-Mo-Bi) from Shanghai Research Institute of Petrochemical Technology (SRIPT), which shows high activity and acrylonitrile selectivity at 380~450 °C. X_m stands for other elements such as Cr, Co, Ni, Mg, Mn and K. The catalyst was synthesized using co-precipitation method, it was then spray dried and calcined in the rotating furnace at the temperature of ~600 °C. Catalytic ammoxidation processes were studied at the Commercial Fluidized Bed Reactor (CFBR) in SPIRT. After 5 to 10 days of its use during the ammoxidation reaction in CFBR, the catalytic activity reached a stable state. Then the catalyst was studied at the accelerating activity-test facilities that employs the Laboratory-scale Fluidized Bed Reactor (LFBR). Using the LFBR, the samples were studied for different times of reaction: fresh (unused), 5 days, 8 days, 11 days, 16 days and 48 days from the

beginning of the reaction. The corresponding samples are denoted as S0, S5, S8, S11, S16 and S48, respectively.

2.2 Raman Spectroscopy

The metal oxide phase present in the MCM catalyst samples was examined using Jobin-Yvon LabRam 1B Raman spectrometer. Before measurement the spectrometer was calibrated using a silicon wafer to a wavelength accuracy of ±1 cm⁻¹. The Raman spectra of the fresh and spent catalysts with different reaction times were then collected under ambient conditions using a 632.8 nm excitation line of He-Ne laser source, equipped with a confocal Olympus microscope (BX-30). The laser power was kept below 0.5 mW at the sample so as to minimize any laser-induced alterations of the sample.

2.3 Diffuse Reflectance UV-vis Spectroscopy

Diffuse reflectance UV-visible spectra of selected samples were carried out (from 12500 to 50000 cm⁻¹) using a Perkin Elmer 555 double beam spectrophotometer at SPIRT. BaSO₄ was used as reference, and slit width was set to 2.0 nm.

2.4 X-ray Absorption Spectroscopy

Fe K-edge X-ray absorption spectroscopy (XAS) data were performed in transmission mode at the beamline X-19A at National Synchrotron Light Source at Brookhaven National Laboratory in New York, USA. Double crystal Si (111) monochromator was detuned 30% to minimize harmonics. Gas-filled ionization chamber detectors were used for measuring incident and transmitted beam intensities. In addition, a third ionization chamber was used to detect the beam through a reference Fe foil, for energy calibration and data alignment purposes. The XAS specimens were made by depositing the catalyst powders onto adhesive tapes and folding the tape several times for homogeneity. The edge steps of the X-ray absorption coefficient at Fe K-edge energy varied between 0.3 and 0.4 for all samples.

Initial data processing was performed by Athena²³ software from IFEFFIT data analysis package. Several consecutive measurements of the same sample, were aligned and averaged to minimize statistical noise in the data. To directly compare X-ray Absorption Near Edge Structure (XANES) data of different samples, the same procedure of pre-edge line fitting, post-edge curve fitting, and edge-step normalization was applied to all samples. Quantitative data analysis was done using PCA software.^{24,25}

3. Results

3.1. Raman spectroscopy

The spectra corresponding to different reaction times are shown in Figure 1. The spectra feature symmetric stretching mode, ν_1 , of the MoO₄ tetrahedron at 955 cm⁻¹, asymmetric stretching mode, at 890 cm⁻¹ and/or 835 cm⁻¹, bending modes in plane and out of plane at 430 and 360 cm⁻¹, and rotation of the entire tetrahedron at 240 cm⁻¹. These observations are in good agreement with literature.²⁶⁻²⁹ Similar spectra have been found in β -CoMoO₄ where $\nu_1=945$ cm⁻¹, Ni/Mo alloys ($\nu_1=940$ cm⁻¹)²⁶, in β -HgMoO₄ ($\nu_1=970$ cm⁻¹), in α -MnMoO₄ ($\nu_1=940$ cm⁻¹), in NiMoO₄ ($\nu_1=960$ cm⁻¹)²⁷. Vibrational modes of MoO₄ have been

reported at 700-900 cm^{-1} and its bending at 300-400 cm^{-1} .²⁸ The spectra shown in Figure 1 also reveal the presence of $\text{Fe}_2(\text{MoO}_4)_3$ in our catalyst, which has a characteristic, high intensity, and well isolated band at 783 cm^{-1} . This in good agreement with reported data for $\text{Fe}_2(\text{MoO}_4)_3$ that feature major bands at 960, 780, and 350 cm^{-1} .^{20,29} Qualitatively, the 783 cm^{-1} peak intensity can thus be used for estimating the amount of $\text{Fe}_2(\text{MoO}_4)_3$ in our catalysts. Figure 1 demonstrates that this compound has exhibited gradual decrease in its quantity with reaction time. Therefore, our Raman measurements, in agreement with previous reports,³⁰ indicate that the major presence of iron exists in the form of $\text{Fe}_2(\text{MoO}_4)_3$ in fresh catalysts (also short service time catalysts) and as its reduction to FeMoO_4 after long-time use. This result is only a partial picture of composition and structure of Fe-Mo phase in the catalyst because other Fe phases that are not Raman-active may also be present.

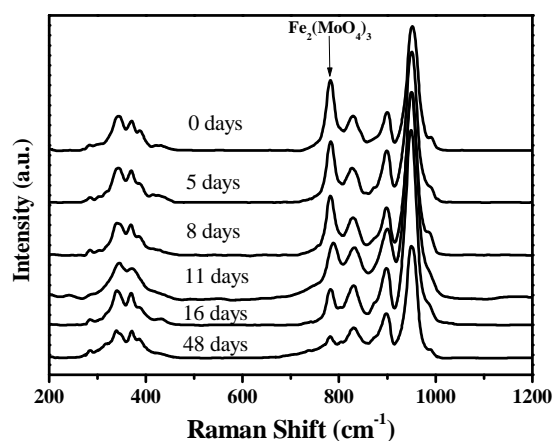


Figure 1 Raman spectra of Fe-Mo-Bi catalysts corresponding to different times after the beginning of the reaction (0, 5, 8, 11, 16, 48 days). Arrow indicates a peak corresponding to the $\text{Fe}_2(\text{MoO}_4)_3$ complex

As demonstrated in Figure 1, $\text{Fe}_2(\text{MoO}_4)_3$ shows abundant load in S0, then decreases monotonically in S5 through S48. For semi-quantitative purposes, the intensity ratio was calculated between the strongest bands from MMoO_4 ($M=\text{Co}, \text{Ni}, \text{Mn}$) and $\text{Fe}_2(\text{MoO}_4)_3$ appearing at $\sim 950 \text{ cm}^{-1}$ and 783 cm^{-1} respectively, if we assume the majority MMoO_4 phases don't change significantly. The values of 0.56, 0.39, 0.35, 0.28, 0.20 and 0.20 for S0, S5, S8, S11, S16 and S48, respectively, demonstrate that $\text{Fe}_2(\text{MoO}_4)_3$ phase has been decomposing during the reaction process, from the highest catalytic activity S0 in the very beginning to the most deactivated sample S48 with the longest service time. We will discuss the reason for this decomposition in greater detail below.

As for the MoO_3 discussed above, it has its characteristic band at 817 cm^{-1} which is clearly missing from the data in Figure 1.³¹ The absence of MoO_3 phase from all samples S0 through S48 is quite reasonable due to their prolonged (5 to 10 days) treatment in CFBR and high volatility of MoO_3 during the reaction process.¹³ As discussed in the Raman characterization section, the amount of $\text{Fe}_2(\text{MoO}_4)_3$ was gradually decreasing with reaction time, but

what exactly happened to $\text{Fe}_2(\text{MoO}_4)_3$ remains unclear. The next section will address this question.

3.2. X-ray Absorption Near Edge Structure

Figure 2 shows Fe K-edge XANES spectra collected in the Fe-Mo-Bi catalysts. The spectra for all samples, from S0 to S48, exhibit gradual shift towards lower energy with the increase of reaction time. By comparing our data with those previously reported^{32,33} we can firmly believe that this trend is consistent with the change in average oxidation state of Fe from +3 towards +2.

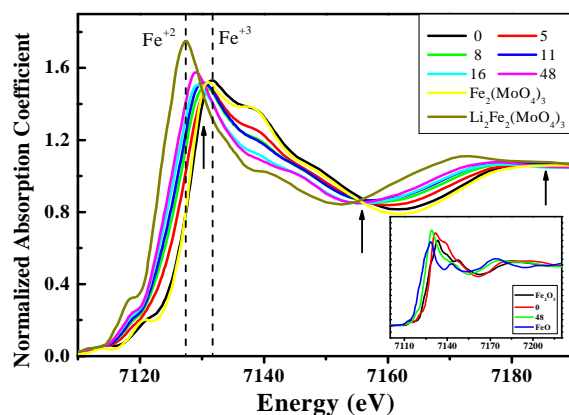


Figure 2 Fe K-edge XANES of Fe-Mo-Bi catalysts with different reaction time, and reference compounds $\text{Fe}_2(\text{MoO}_4)_3$, $\text{Li}_2\text{Fe}_2(\text{MoO}_4)_3$, Fe_2O_3 and FeO . Arrows show presence of quasi-isosbestic points indicating both the one-step transformation within the catalysts from S0 towards S48 and their agreement with the two standards ($\text{Fe}_2(\text{MoO}_4)_3$, and $\text{Li}_2\text{Fe}_2(\text{MoO}_4)_3$)

Figure 2 and its inset show dramatic changes in the Fe K-edge XAS data for different stage catalysts, and reference compounds $\text{Fe}_2(\text{MoO}_4)_3$, $\text{Li}_2\text{Fe}_2(\text{MoO}_4)_3$, Fe_2O_3 and FeO . The catalyst data and the $\text{Fe}_2(\text{MoO}_4)_3$, $\text{Li}_2\text{Fe}_2(\text{MoO}_4)_3$, and Fe_2O_3 references were obtained in two different experiments (the reference compounds were measured by Shirakawa, et al³²). In order to directly compare them, all data were first aligned in absolute energy using reference data of Fe foil (in the case of the catalyst samples) and Fe_2O_3 (in the case of $\text{Fe}_2(\text{MoO}_4)_3$ and $\text{Li}_2\text{Fe}_2(\text{MoO}_4)_3$ data) measured simultaneously with all the samples. By measuring the XAFS data in Fe foil and Fe_2O_3 in the same transmission experiment we obtained the relative shifts needed to apply for all data sets to share the same X-ray energy origin.

Nearly perfect agreement between the starting sample, S0, and $\text{Fe}_2(\text{MoO}_4)_3$ demonstrate that: 1) the charge state of Fe ion was +3 in the fresh catalyst, and 2) its Fe phase was predominantly $\text{Fe}_2(\text{MoO}_4)_3$. The absorption edge positions are defined as the main absorption peak maxima throughout this article. For the $\text{Fe}_2(\text{MoO}_4)_3$ and S0 data, the Fe K-edge positions were at 7131.8 eV and 7131.5 eV, respectively. Upon catalytic reaction for some period of time, the spectra shift to lower energies, towards the reduced form of the iron molybdate, FeMoO_4 with the charge state of Fe to +2. Instead of measuring FeMoO_4 , we compare our data with another Fe^{+2} compound of $\text{Li}_2\text{Fe}_2(\text{MoO}_4)_3$ ³⁴ which has the same local structure around Fe as in the FeMoO_4 .³⁵ As shown

in Table 1, not only the distributions of the first shell Fe-O distances and the second shell Fe-Mo distances around Fe, but also the coordination environment in these two compounds are very similar. Hence, the use of the $\text{Li}_2\text{Fe}_2(\text{MoO}_4)_3$ for comparing with experimental data in the Fe-Mo-Bi catalysts is justified.

Table 1 Relevant Structure Parameters of FeMoO_4 ³⁵ and $\text{Li}_2\text{Fe}_2(\text{MoO}_4)_3$ ³⁴

Fe environment	FeMoO_4	$\text{Li}_2\text{Fe}_2(\text{MoO}_4)_3$	difference
Charge valence	+2	+2	0
Fe-O coordination number	6	6	0
Fe-Mo coordination number	6	6	0
Average Fe-O distance (Å)	2.14	2.12	< 1 %
Average Fe-Mo distance (Å)	3.61	3.67	< 2 %

In the spectra of the last sample, S48, its Fe K-edge energy (7129 eV) was higher than that of $\text{Li}_2\text{Fe}_2(\text{MoO}_4)_3$ (7127 eV), as shown in Figure 2. Hence, the average charge state of Fe in the last sample is not equal to, but approaching the value of +2. As evidenced by the presence of quasi-isosbestic points in Figure 2, Fe ions in all samples undergo transformation from ferric molybdate to ferrous molybdate other than iron oxide FeO, since its spectroscopic features are different from both S0 and S48.

One possible method of quantitative analysis of these XANES spectra is by linear combination analysis. In this method, data are represented as a linear combination of two or more standard compounds and their mixing fractions correspond to the volume fractions of the corresponding iron species in the sample. The problem with this method is that, it does not offer a model-independent determination of the number of independent species. Principal Component Analysis (PCA) is a superior method for that purpose, because it allows to 1) find the number of independent species mixed together in the sample at all reaction times and 2) obtain their unique identities.^{25,36}

Figure 3 (a) shows the “scree test”, demonstrating that the number of principal components required to reproduce all 6 experimental spectra is equal to 2, as evidenced by the negligible Eigenvalue (0.005) there. The standard compounds of $\text{Fe}_2(\text{MoO}_4)_3$ and $\text{Li}_2\text{Fe}_2(\text{MoO}_4)_3$ were well reproduced by the combination of the two principal components and the target transform was performed from the basis of abstract components to the basis corresponding to the two standards. The mixing fraction of the Fe +3 and Fe +2 states was obtained using linear combination fit that was using the PCA software package.³⁷ Data reproduction of the experimental spectra and two standards is shown in Fig. 3 (b) as an example.

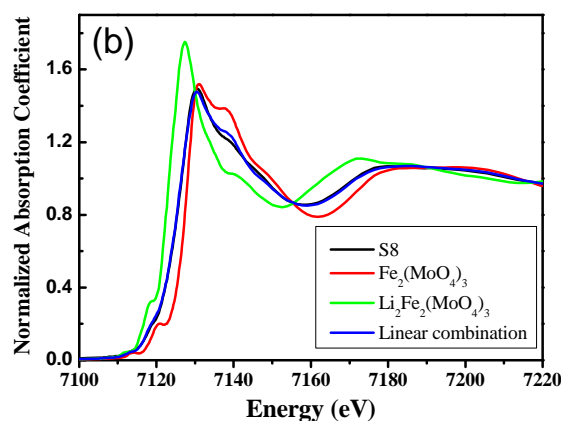
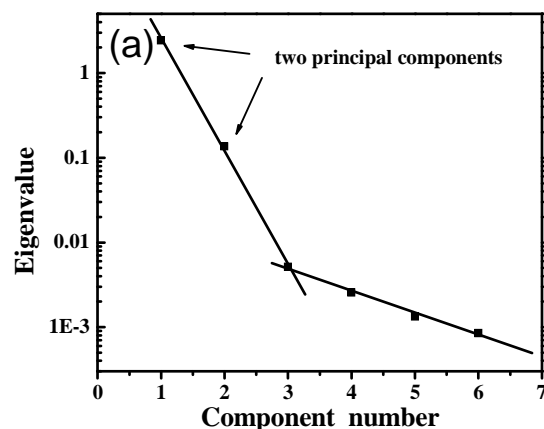


Figure 3 (a) The “scree test” shows the change trend of the eigenvalues obtained by Principal Component Analysis. The change in slope after two leading eigenvalues indicates that the number of independent species in the sample is equal to 2; (b) Representative linear combination fit of the sample S8 using the standard ends of $\text{Fe}_2(\text{MoO}_4)_3$ and $\text{Li}_2\text{Fe}_2(\text{MoO}_4)_3$. The mixing fraction of them was the only fitting variable

We have also tested a three-species model against our experimental data, using Fe_2O_3 as a possible standard, in addition to the previous two-species standards as described above. The best fit values of the mixing fractions, corresponding to species after the target transform procedure, had large negative values, which is non-physical. Hence, our XANES data give no evidence for formation of Fe_2O_3 , within the accuracy of the PCA method used.

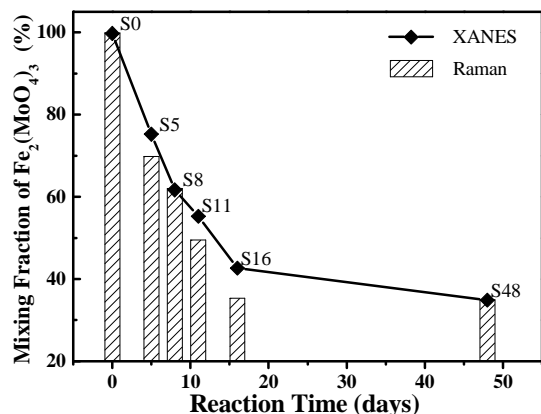


Figure 4 Fractions of $\text{Fe}_2(\text{MoO}_4)_3$ in the samples S0 through S48 obtained using two different characterization methods, Raman and XANES, exhibit similar trends. The two measurements indicate that the amount of $\text{Fe}_2(\text{MoO}_4)_3$ has decreased with reaction time

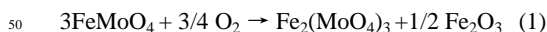
Guided by the PCA results, we treat the changes of Fe oxidation state in the catalyst during the reaction as a one-step transformation from Fe^{+3} to Fe^{+2} , and summarize the quantitative information about the rate of this transformation in Figure 4. The best fit results for samples 0, 5, 8, 11, 16 and 48 show gradual and monotonic decrease of the fraction of $\text{Fe}_2(\text{MoO}_4)_3$ from 99% to 37%. According to these results, the average Fe charge states in all samples as varying from +3 at S0 to +2.37 in S48. This result demonstrates that the average Fe oxidation state in all spent catalysts, even for the longest reaction time, is still much higher than +2 which is the oxidation state of Fe in FeMoO_4 .

Due to the ensemble-averaging nature of XAFS, there are two models that can be used to interpret the PCA results: 1) A “homogeneous transformation”, in which every Fe atom changes its charge state from +3 towards +2.37 for sample S0 towards sample S48, and 2) “Heterogeneous transformation”, where Fe atoms are divided in two groups at all times, with charge states of +3 and +2, with volume fractions x and $1-x$, respectively. The volume fraction of Fe^{3+} changes from 99% to 37% for samples S0 to S48, respectively. Both models will give identical XANES trends and identical results in linear combination analysis. Hence, within the results of just one technique, XANES, it is impossible to differentiate between the two models. However, Raman spectra show that Fe^{3+} , in particular, $\text{Fe}_2(\text{MoO}_4)_3$ remains in all the samples through different reaction stages, not only in the fresh catalyst S0 but also in the last one S48. That observation is consistent with model 2) and inconsistent with model 1). Thus, the combination of XAFS and Raman measurements is required to validate a hypothesis of partial $\text{Fe}_2(\text{MoO}_4)_3$ transformation, specifically $\text{Fe}_2(\text{MoO}_4)_3 \rightarrow \text{FeMoO}_4$ during the selective ammoxidation process. This transformation will be discussed in greater detail below.

3.3. UV-vis diffuse reflectance spectroscopy

Figure 5 shows the DR-UV-vis spectra of selected samples from Fe-Mo-Bi catalysts with different reaction times. All the spectra exhibit a characteristic absorption band of $\text{Fe}_2(\text{MoO}_4)_3$ at

$\sim 460 \text{ nm}$.^{12,38} The broad absorption in the UV region is ascribed to the presence of both tetrahedral and octahedral oxomolybdate groups,³⁹ whereas the one in visual region is attributed to Fe_2O_3 .⁴⁰ This iron oxide becomes increasingly abundant, accompanied by catalyst sample showing red-brown color characteristic of the fresh Fe_2O_3 ,⁴¹ with longer reaction times according to either or both of these mechanisms:



Taking into account the different crystal structures of α - and β - FeMoO_4 phases (Mo^{6+} coordination is octahedral in α and tetrahedral in β), it is reasonable to conclude that the mechanism (1) occurs preferentially for β phase and (2) for α phase, as Mo^{6+} coordination is tetrahedral in $\text{Fe}_2(\text{MoO}_4)_3$ but octahedral in MoO_3 . Given that no MoO_3 was detected in the Raman spectra from S0 through S48, one can further conclude that Eq. 1 is the main reoxidation path during the entire catalytic process. As a result, Eq. 1 will lead to more stable catalytic activities than Eq. 2, due to the regeneration of $\text{Fe}_2(\text{MoO}_4)_3$. As for the increasingly accumulating Fe_2O_3 , as evidenced by the UV-Vis spectra (Fig. 5), its absence in Raman spectra and in the Fe K-edge XANES spectra indicates that it is present in the sample as a minority Fe species whose volume fraction does not exceed ca. 5%, which is the uncertainty in the Fe speciation by Principal Component Analysis of XANES spectra.

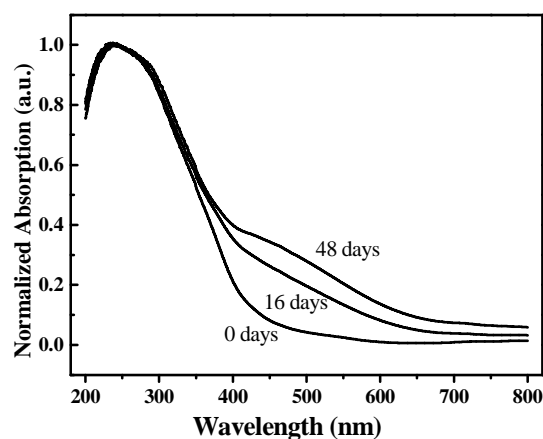
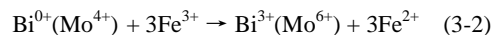


Figure 5 Diffuse reflectance UV-visible spectra of selected Fe-Mo-Bi catalyst samples. The data are normalized by the absorption maximum. The increasing intensity in the region between 400 and 700 nm shows the growing amount of Fe_2O_3 with reaction time.

4. Discussion

As well documented elsewhere,^{42,43} propylene ammoxidation obeys Mars-Krevelen mechanism and is a six-electron redox process.⁴⁴ Iron molybdate, both ferric- and ferrous-one, is a good example for efficient redox couple. It can promote air dioxygen dissociation on Fe^{2+} into lattice oxygen $[\text{O}]_L$, and its transfer to the active site using Fe^{3+} .⁴⁵ The latter, in turn, will reoxidize the

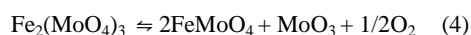
resulting reduced Bi and Mo^{10,46}, further turning C₃H₆ into target product C₃H₃N as well:



It is evident from these examples that iron molybdate is an active species throughout the entire catalytic reaction and has played crucial roles in the ammoxidation process. For the sake of high performance on Fe-Mo-Bi catalyst, the balance between Fe³⁺ and Fe²⁺ should be kept close to that in the initial state, which is known to have the highest catalytic activity and selectivity.⁴⁷ Our experiment demonstrated (Figure 1), that the initial state of the iron molybdate, Fe₂(MoO₄)₃, has decomposed significantly for all catalyst samples from S5 through S48. The rate of decomposition was the fastest during the first 16 days catalytic process.

XAS results not only have illuminated the time-dependent decomposition of the iron molybdate during the reaction, but also have revealed that iron-containing phase in fresh sample S0 is predominantly Fe₂(MoO₄)₃. In addition, the combined use of Raman and XAS helped us to propose the deactivation mechanism for Fe₂(MoO₄)₃, which follows the Fe₂(MoO₄)₃ → FeMoO₄ step. Another important result emerging from this work is that Fe³⁺ directly transforming towards Fe²⁺, with no intermediate phase. During this transformation, the volume fraction of Fe³⁺ changes from 100 to 37% for samples S0 to S48 respectively, and the volume fraction of Fe²⁺ increases accordingly. While speciation of chemical states of iron has been made possible by XAS in earlier works,^{48,49} it is due to the complementarity of XAS and Raman experiments that such conclusion can be made in the present case. Each technique, taken alone, will only show an incomplete picture.

We now turn our attention to the possible origins of decomposition of Fe₂(MoO₄)₃. The following equation is a plausible description of the process:



For an ideal catalyst, iron molybdate could strike a balance between its ferric and ferrous forms during the catalysis process, and the balance should be fully reversible. In that case, the catalytic activity of the spent catalyst, e.g., conversion of propylene, will be same as the fresh one. However, due to the loss of MoO₃ via volatilization and much easier sublimation of MoO₂(OH)₂ after combination with resulting H₂O (Eq. 3),⁵⁰ Eq. 4 loses its reversibility. Therefore, ferrous molybdate can only partially get oxidized and restored back to Fe₂(MoO₄)₃ incompletely, resulting in increasing amount of resultant FeMoO₄. We propose that Eq. 1 is the likely oxidation route because no MoO₃ was detected by Raman spectra (Figure 1) and it is accompanied by small amount of Fe₂O₃ which was detected by DR-UV-Vis (Figure 5). The presence of a minute amount of iron oxide is not in contradiction with our XAS results because the uncertainties in the LCA-derived error bars on mixing fractions allow for 5 % of another iron species in the sample (*vide supra*), and UV-vis is highly sensitive to Fe₂O₃. Hence, role of the UV-vis measurement was very important here because,

without it, the presence of Fe₂O₃ could not have been detected.

In conclusion of all the observations described above, we find that continuously increasing accumulation of FeMoO₄ and depletion of Fe₂(MoO₄)₃ is inevitable with the increased reaction time, provided that no additional MoO₃ is added to the reaction mixture to reverse the Eq. 4 towards the Fe₂(MoO₄)₃ direction. As a result, the catalytic performance of Fe-Mo-Bi catalyst, will degrade with reaction time.

Two recommendations for rationally designing better ammoxidation catalysts emerge from our findings. First, it is important to maintain a sufficient number of Fe³⁺ sites in an overall reducing atmosphere (propylene ammoxidation to acrylonitrile), it is necessary to stabilize the Fe³⁺ state structurally and/or functionally. One candidate for such stabilizer is the Cr³⁺/Cr²⁺ redox couple. It is, generally more effective at higher temperature than iron couple,⁴³ in addition, it acts as a structural diluents to iron and booster of the Fe³⁺ state in Fe-Mo-Bi matrix. Relevant tests are presently under way in our group and will be reported elsewhere. Second, it is important to replenish the MoO₃ into the reacting mixture, to compensate for its loss through volatilization or sublimation as to slowing down the collapse of ferric molybdate. The MoO₃ may come from a separate component compound or some other compound as suggested elsewhere.^{5,6}

Based on the discussion stated above, we conclude that ideal Fe-Mo-Bi catalysts for AN ammoxidation should be both functionally and structurally stable. The former requires, using iron molybdate as a key component and an example, that its functional form be kept the same as in the fresh catalyst. Based on our results, and the work of others, a revised feasible model for highly active and long-term stable Fe-Mo-Bi catalyst may be proposed, as illustrated in Figure 6. In this catalyst the Fe³⁺/Fe²⁺ redox couple is crucial, both composing reversible redox processes and stabilizing the main structure of catalysts by suppressing its deformation, due to active component decomposition.

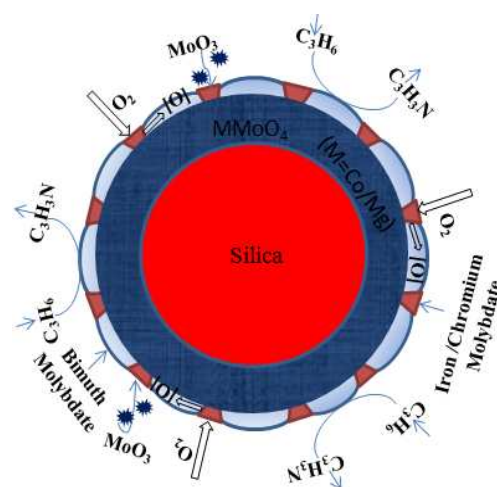


Figure 6 Schematic model for Fe-Mo-Bi catalyst, shows the role of Fe³⁺/Fe²⁺ redox couple during the propylene catalytic ammoxidation process. Propylene C₃H₆ are converted into target compound C₃H₃N on bismuth molybdate through H-abstraction and lattice O-incorporation,

while iron molybdate (including ferric- and ferrous-) acts as dioxygen dissociation and lattice oxygen transfer. Two highlighted strategies proposed here, are the introduction of $\text{Cr}^{3+}/\text{Cr}^{2+}$ redox couple in the catalyst preparation, and replenishment of MoO_3 via separate component or compound during the reaction process

5. Summary and conclusions

In our Fe-Mo-Bi catalysts, an iron molybdate phase identified as $\text{Fe}_2(\text{MoO}_4)_3$ has undergone dramatic partial (more than 60%) decomposition with reaction time. This decomposition was a one-step transformation from the Fe^{3+} into another form of iron molybdate, namely FeMoO_4 with the iron charge state of +2. These results were obtained by a combination of Raman spectroscopy and XANES spectroscopy studies of the fresh and spent catalysts at different reaction times. DR-UV-vis measurements revealed a small fraction (less than 5 volume %) of Fe_2O_3 during the reaction process. The combination of these measurements allowed us to propose mechanism of transformation of iron molybdate and its role in the propylene ammoxidation process. This work highlights the critical role of Fe^{3+} species for the stable and efficient conversion of propylene to acrylonitrile in the selective ammoxidation. A modification of the Fe-Mo-Bi catalyst that will help stabilize Fe^{3+} ions is proposed.

Acknowledgements

AIF acknowledges support from the Chemical Sciences, Geosciences, and Biosciences Division, Office of Basic Energy Sciences, Office of Science, U. S. Department of Energy, Grant No. DE-FG02-03ER15476. Use of the NSLS is supported by the U.S. Department of Energy, Office of Science, Office of Basic Energy Sciences, under Contract No. DE-AC02-98CH10886. Beamline X19A at the NSLS is supported in part by the Synchrotron Catalysis Consortium, U.S. Department of Energy Grant No. DE-FG02-05ER15688. We are grateful to Drs. Yuanyuan Li and Nebojsa Marinkovic for their help with synchrotron measurements.

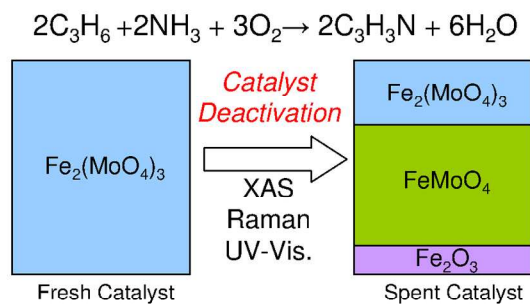
Notes and references

^a Shanghai Research Institute of Petrochemical Technology, 1658 Pudong Beilu, Shanghai 201208, China. E-mail: yangwm.sshy@sinopec.com
^b Physics Department, Yeshiva University, New York, NY 10016 USA. E-mail: anatoly.frenkel@yu.edu

- 1 R. Grasselli, J. Burrington, D. Buttrey, P. DeSanto, Jr., C. Lugmair, A. Volpe, Jr. and T. Weingand, *Top. Catal.*, 2003, **23**, 5-22.
- 2 R. K. Grasselli, Proceedings of the DGMK Conference, 2001, Hamburg, Germany p.147
- 3 T. S. R. P. Rao and K. R. Krishnamurthy, *J. Catal.*, 1985, **95**, 209-219.
- 4 R. K. Grasselli and H. F. Hardman, U. S. Patent 3642930 (1972).
- 5 R. K. Grasselli, D. D. Suresh and H. F. Hardman, U. S. Patent 4001317 (1977); U. S. Patent 4167494 (1979).

- 6 G. W. Keulks, L. D. Krenzke and T. M. Notermann, in *Advances in Catalysis*, eds. H. P. D.D. Eley and B. W. Paul, Academic Press, 1979, v. 27, pp. 183-225.
- 7 I. B. Annenkova, T. G. Alkazov and M. S. Belenku, *Kinet. Catal.* 1969, **10**, 1305-1311.
- 8 P. A. Batist, C. G. M. van de Moesdijk, I. Matsuura and G. C. A. Schuit, *J. Catal.*, 1971, **20**, 40-57.
- 9 M. W. J. Wolf, Ph.D. thesis "Selective Oxidation of Olefins over Multicomponent Molybdate Catalysts". Technische Hoge School, Eindhoven 1974; I. Matsuura and M. W. J. Wolfs, *J. Catal.*, 1975, **37**, 174-178.
- 10 P. A. G. Van Oeffelen, Ph.D. thesis "Selective Oxidation of Olefins on Molybdate Catalysts". Technische Hoge School, Eindhoven 1978
- 11 P. A. Batist, *Surf. Technol.*, 1979, **9**, 443-446.
- 12 M. W. J. Wolfs and P. H. A. Batist, *J. Catal.*, 1974, **32**, 25-36.
- 13 A. P. V. Soares, M. F. Portela, A. Kiennemann and L. Hilaire, *Chem. Eng. Sci.*, 2003, **58**, 1315-1322.
- 14 N. Pernicone, *Catal. Today*, 1991, **11**, 85-91
- 15 N. Burriesci, F. Garbassi, M. Petrala, G. Petrini and N. Pernicone, in *Studies in Surface Science and Catalysis*, eds. B. Delmon and G. F. Froment, Elsevier, 1980, v. 6, pp. 115-126
- 16 S. Bordiga, E. Groppo, G. Agostini, J. A. van Bokhoven and C. Lamberti, *Chem. Rev.*, 2013, **113**, 1736-1850; I. E. Wachs and C. A. Roberts, *Chem. Soc. Rev.*, 2010, **39**, 5002-5017.
- 17 R. A. Schoonheydt, *Chem. Soc. Rev.*, 2010, **39**, 5051-5066; F. Cesano, S. Bertarione, A. Piovano, G. Agostini, M. M. Rahman, E. Groppo, F. Bonino, D. Scarano, C. Lamberti, S. Bordiga, L. Montanari, L. Bonoldi, R. Millini and A. Zecchina, *Catal. Sci. Technol.*, 2011, **1**, 123-136.
- 18 G. Waychunas, M. Apter and G. Brown, Jr., *Phys Chem Minerals*, 1983, **10**, 1-9.
- 19 A. Patlolla, P. Baumann, W. Xu, S. D. Senanayake, J. A. Rodriguez and A. I. Frenkel, *Top. Catal.*, 2013, **56**, 896-904.
- 20 Q. Xu, G. Jia, J. Zhang, Z. Feng and C. Li, *J. Phys. Chem. C*, 2008, **112**, 9387-9393.
- 21 R. K. Grasselli, *Cat. Today*, 1999, **49**, 141 R. K. Grasselli, *App. Catal.*, 1985, **15**, 127-139.
- 22 D. D. Suresh, M. S. Friedrich, M. J. Seely, U. S. Patent 5212137 (1993); O. V. Udalova, D. P. Shashkin, M. D. Shibanova and O. V. Krylov, *Kinet. Catal.*, 2005, **46**, 535-544.
- 23 B. Ravel and M. Newville, *J. Synchrotron Radiat.*, 2005, **12**, 537-541.
- 24 S. R. Wasserman, *J. Phys. IV France*, 1997, **7**, C2-203-205.
- 25 A. I. Frenkel, O. Kleinfeld, S. R. Wasserman and I. Sagi, *J. Chem. Phys.*, 2002, **116**, 9449-9456.
- 26 P. Delichere, A. Hugot-Le Goff and S. Joiret, *Surf. Interface Anal.*, 1988, **12**, 419-423.
- 27 I. Kanesaka, H. Hashiba and I. Matsuura, *J. Raman Spectr.*, 1988, **19**, 213-218.
- 28 H. Tian, I. E. Wachs and L. E. Briand, *J. Phys. Chem. B*, 2005, **109**, 23491-23499; I. Matsuura, R. Schut and K. Hirakawa, *J. Catal.*, 1980, **63**, 152-166.
- 29 G. Hill Jr and J. H. Wilson III, *J. Mol. Catal.*, 1990, **63**, 65-94.
- 30 X. Ge, J. Shen and H. Zhang, *Science in China B*, 1996, **39**, 53-63.
- 31 M. Dieterle, G. Weinberg and G. Mestl, *Phys. Chem. Chem. Phys.*, 2002, **4**, 812-821.
- 32 J. Shirakawa, M. Nakayama, M. Wakihara and Y. Uchimoto, *J. Phys. Chem. B*, 2007, **111**, 1424-1430.
- 33 A. M. Beale, S. D. M. Jacques, E. Sacaliuc-Parvaescu, M. G. O'Brien, P. Barnes and B. M. Weckhuysen, *Appl. Catal. A: General*, 2009, **363**, 143-152.
- 34 C. C. Torardi and E. Prince, *Mat. Res. Bulletin*, 1986, **21**, 719-726
- 35 A. W. Sleight, B. L. Chamberland and J. F. Weiher, *Inorg. Chem.*, 1968, **7**, 1093-1098.
- 36 J. Y. Kim, J. A. Rodriguez, J. C. Hanson, A. I. Frenkel and P. L. Lee, *J. Am. Chem. Soc.*, 2003, **125**, 10684-10692.
- 37 S. R. Wasserman, P. G. Allen, D. K. Shuh, J. J. Bucher and N. M. Edelstein, *J. Synchrotron Radiat.*, 1999, **6**, 284-286.

- 38 P. Forzatti, P. L. Villa, N. Ferlazzo and D. Jones, *J. Catal.*, 1982, **76**, 188-207.
- 39 W. D. Kovats and C. G. Hill, *Appl. Spectrosc.*, 1986, **40**, 1215-1223.
- 40 A. C. Scheinost, A. Chavernas, V. Barron and J. Torrent, *Clays and Clay Minerals*, 1998, **46**, 528-536.
- 41 Z. Zhang, M. F. Hossain and T. Takahashi, *App. Catal. B: Environ.*, 2010, **95**, 423-429.
- 42 R. K. Grasselli, *J. Chem. Ed.*, 1986, **63**, 216-221.
- 43 P. Mars and D. W. van Krevelen, *Chem. Eng. Sci.*, 1954, **3**, 41-59.
- 44 R. K. Grasselli, Ammoxidation, in "Handbook of Heterogeneous Catalysis" (v. 5) p. 2302. G. Ertl, J. Weitkamp, and H. Knoezinger, Eds. John Wiley & Son Inc., New York (1997)
- 45 R. K. Grasselli, *Cat. Today*, 1999, **49**, 141-153.
- 46 R. Schlögl, A. Knop-Gericke, M. Hävecker, U. Wild, D. Frickel, T. Ressler, R. E. Jentoft, J. Wienold, G. Mestl, A. Blume, O. Timpe and Y. Uchida, *Top. Catal.*, 2001, **15**, 219-228.
- 47 A. A. Firsova, Y. V. Maksimov, V. Y. Bychkov, O. V. Isaev, I. P. Suzdalev and V. N. Korchak, *Kinet. Catal.*, 2000, **41**, 116-121.
- 48 E. Borfecchia, L. Mino, D. Gianolio, C. Groppo, N. Malaspina, G. Martinez-Criado, J. A. Sans, S. Poli, D. Castelli and C. Lamberti, *J. Anal. At. Spectrom.*, 2012, **27**, 1725-1733.
- 49 G. Berlier, G. Spoto, S. Bordiga, G. Ricchiardi, P. Fiscaro, A. Zecchina, I. Rossetti, E. Selli, L. Forni, E. Giamello and C. Lamberti, *J. Catal.*, 2002, **208**, 64-82.
- 50 L. Zhang, D. Liu, B. Yang and J. Zhao, *App. Catal. A: General*, 1994, **117**, 163-171.



Combination of X-ray absorption, Raman and UV-visible spectroscopies reveals competing redox reactions during deactivation of Fe-based complex catalysts
297x209mm (150 x 150 DPI)